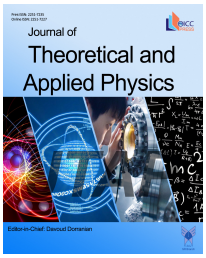

Volume 19, Issue 5, 192550 (1-10)

Journal of Theoretical and Applied Physics (JTAP)

https://doi.org/10.57647/j.jtap.2025.1905.50

Enhanced visible-light photocatalytic activity of Ag-WO_3/cement composites for organic pollutant removal

Ban Mazin Alshabander[1,*], Safaa Ahmed Al-Lhaibi[2]

[1]*Department of Physics, College of Science, University of Baghdad, Baghdad, Iraq.*
[2]*Ministry of Education, Baghdad, Iraq.*

[*]**Corresponding author:** ban.muzahem@sc.uobaghdad.edu.iq

Original Research

Received:
30 June 2025
Revised:
24 August 2025
Accepted:
4 September 2025
Published online:
31 October 2025

Abstract:

This research focused on creating a practical cement composite with self-cleaning abilities by embedding silver-doped tungsten trioxide (Ag-WO_3) nanoparticles. We made several composites with different amounts of silver (0, 5, 7, and 15 wt.%) using a straightforward molding process. To understand the materials we created, we used techniques like X-ray diffraction (XRD), scanning electron microscopy (SEM), and UV-Vis spectroscopy. The XRD results confirmed that the WO_3 in our composites had a monoclinic crystal structure, while SEM imaging showed that the nanoparticles were spread evenly across the cement surface. Furthermore, UV-Vis analysis proved that adding silver caused a redshift, meaning the material became better at absorbing visible light by reducing its bandgap energy. The most important finding was that the amount of silver added made a huge difference in performance. The composite with 7% Ag-WO_3 was by far the most effective. When tested under natural sunlight, it broke down 89% of a methylene blue dye pollutant in just 40 minutes. We believe this boost in performance happens because the silver particles, at this optimal amount, are perfectly dispersed and act as tiny electron traps, preventing energy waste and maximizing the photocatalytic reaction. However, adding too much silver (15%) caused the particles to clump together, which blocked light and made the composite less effective. In the end, our results show that embedding 7 wt.% Ag-WO_3 into cement is a highly effective strategy for producing smart, self-cleaning building materials that can help tackle environmental pollution.

Keywords: Ag-WO_3; Photocatalytic activity; Cement; Nanocomposites; Self-cleaning

1. Introduction

The long-term development of cities is increasingly constrained by the severe challenges of environmental contamination [1–3]. Pollution from industrial waste gases and wastewater, as well as automobile exhaust, runoff, and waste from routine cleanup procedures endanger the urban environment and human health. In this context, self-cleaning surfaces represent an excellent technological tool for living a more environmentally conscious life [4, 5].

Portland cement, a fundamental building block of modern infrastructure, consists of calcium, iron, silica, aluminum, and other minerals in carefully controlled trace amounts. Ironically, the cement industry itself is one of the main causes of air pollution, which is very worrying [6, 7]. A composite material is formed by combining two or more distinct components to form an entirely new compound of higher quality, based on the desired properties. Cement and aggregate are combined to form concrete, which is easier to form than pieces of rock but is just as strong. At the microscopic scale, interfacial interactions between phases are critical in complex mixtures. This is critical for the newly emerging class of materials known as nanocomposites. The incorporation of nanomaterials, which are multiphase solids with unusual physical properties, during the manufacturing process can significantly enhance material performance and has a wide range of uses. The volume ratio of nanoparticles added is very low due to the large surface area to volume ratio of nanoparticles [8].

This study is important because it addresses a dual environmental challenge: It seeks to mitigate pollution using the very material (cement) that contributes to it, thereby adding value and functionality to a ubiquitous construction material. By developing photocatalytic cement composites, we can transform passive structures into active, pollution-fighting assets.

Photocatalytic technology is one of the best strategies for controlling air contamination and in the aquatic environ-

ments and wastewater to remove micropollutants from surfaces through oxidation methods. Simply put, the catalyst in the process accelerates the photoreaction by activating the photocatalyst with UV radiation or solar light. Electron-hole pairs are produced when optical radiation has an energy value equal to or greater than the band gap energy, causing an electronic transition from the valence band to the conduction band. The catalytic reaction is used to oxidize organic compounds and degrade most organic pollutants. This method can significantly accelerate the biodegradation process of highly degradable chemicals during the pretreatment stage. The process of photocatalytic activity is exceptional, given the economic cost, keeping the environment and surfaces free of dirt and pollutants [9–13]. As a result, a number of variables may affect how well the photocatalytic activity is determined [14], including the catalyst's surface characteristics and the reaction medium's conditions.

Among various semiconductors, metal oxide semiconductors, including TiO_2, ZnO, WO_3, and others, have shown strong photocatalytic activity in the conversion of hazardous organic pollutants into innocuous molecules like CO_2 and H_2O when exposed to light [15, 16]. For this study, tungsten trioxide (WO_3) was selected as the primary photocatalyst due to its several advantageous properties over the more commonly used TiO_2. It is a non-toxic, chemically stable, inexpensive n-type semiconductor that absorbs a larger portion of solar radiation because of its narrower energy gap of $2.4 - 2.8$ eV. Its strong response capabilities, physical properties, chemical composition, and ability to be activated by visible light irradiation make it a desirable choice for photocatalysis research [17–21]. Strong solar spectrum absorption, stable chemical and physical characteristics, strong resistance to photo corrosion, and a deep valence band (VB) are just a few of the many benefits of this semiconductor material [22, 23]. At pH $= 0$, WO_3 has a conduction band $E_{CB} = +0.4$ V vs NHE. For the oxidation of water to oxygen, holes in the valence band at $E_{VB} = +3.1$ V are ideal [24–27].

To further enhance the photocatalytic efficiency of WO_3, silver (Ag) was chosen as a dopant. Silver nanoparticles are renowned for their surface plasmon resonance effect, which can dramatically increase light absorption in the visible range. Furthermore, silver acts as an effective electron sink, capturing photogenerated electrons from WO_3 and thus reducing the recombination rate of electron-hole pairs, which is a critical factor for boosting photocatalytic activity. Photo cement-based composites are effective in reducing urban pollution and have aroused widespread interest among academics [28, 29]. Nowadays, they are utilized in the construction of metropolitan roadways, interior materials, and external walls. One practical technique for eliminating organic contaminants from water is photocatalysis, which uses sun energy. It is among the most practical and successful strategies for addressing the enormous issue of environmental pollution [25]. Semiconductor oxides are fascinating, affordable, and safe for both the environment and humans. These properties make it ideal for photocatalysis [30].

Despite the potential of Ag-WO_3, its integration into cementitious matrices for large-scale self-cleaning applications presents specific challenges. Current research lacks a systematic optimization of Ag doping levels to balance between enhanced charge separation and the detrimental effects of nanoparticle agglomeration. Furthermore, a clear understanding of the structure-activity relationship within the complex cement environment under natural sunlight is needed.

Therefore, this research aims to develop a photocatalytic cement composite with self-cleaning properties by embedding tungsten trioxide nanoparticles doped with silver at a ratio of (0, 5, 7, and 15 wt.%) Ag- WO_3 within the cement matrix. The study will involve synthesizing these Ag-WO_3 particles and incorporating them at various loading concentrations into cement using a direct consolidation method to create practical and scalable materials. The effectiveness of the resulting composites will be evaluated by testing their ability to catalyze the degradation of methylene blue, a common organic dye, under natural sunlight. Furthermore, a detailed microstructural analysis will be performed to understand how the additive interacts with the cement and to identify the optimal nanoparticle loading that yields the highest photocatalytic activity for environmental remediation applications.

2. Materials and methodology

2.1 Materials

Materials used in this study were, tungsten trioxide nanoparticles (WO_3) having a $40 - 60$ nm average particle size, yellow color, 99.9% purity from Hongw International Group Company, China. Silver nitrate powder ($AgNO_3$) was purchased from Fisher Scientific, UK with purity 99.8%. Iraqi Ordinary Portland Cement, or Tasluja as it is known commercially, to prevent moisture absorption, the cement was stored in a dry atmosphere. Natural Sand, deionized water and tap water were also used in this study. The experiment used Methylene blue (MB) as organic model of pollutant obtained from CDH in India. MB was selected for this study due to its well-characterized photocatalytic degradation pathway, its widespread use as a standard organic dye pollutant for evaluating photocatalytic activity, and its strong absorption in the visible region, which facilitates straightforward monitoring of degradation kinetics via UV-Vis spectroscopy

2.2 Composite preparation

To prepare Ag-WO_3/cement composite samples, different amounts of silver nitrate powder were dissolved in water to form a silver nitrate solution. 1 g of WO_3 nanoparticles were added to solution of silver nitrate by using ultrasonication for 30 minutes in a dark environment. The different weight percentages of Ag to WO_3 were (0, 3, 5, 7 and 15% wt.) respectively. Then, the Ag-WO_3 solution was mixed with the cement mortar mixture. The Ag-WO_3 additive was incorporated at a loading of 0.5% by weight of the cement. The mixture was stirred for 5 min, then poured into 60 mm diameter glass molds and allowed to cure for 24 to 48 hours at room temperature (25 ± 2 °C). After demolding, all specimens were cured by spraying with water for 3 days

to ensure proper hydration.
The ratio of cement, sand adds to water 1:2:0.5 to prepare a pure sample. Each Ag-WO_3/cement composite sample that was examined had a diameter of 60 mm, a thickness of 5 mm, and a weight of 35 g.

2.3 XRD analysis

X-ray diffraction (XRD) analysis was performed using a Malvern Panalytical X′Pert Pro diffractometer (Model: X′Pert Pro, Malvern Panalytical, Netherlands). The test was conducted with Cu Kα radiation ($\lambda = 1.5406$ Å) at 40 mA and 45 kV. The scanning range was from 10° to 80° (2θ) with a step size of 0.026° and a scanning rate of 1° per minute. The analysis was performed in Baghdad, Iraq.

2.4 Scanning electron microscopy (SEM)

The scanning electron microscope (SEM) has a very important role in determining the shape of surfaces and the parts that make them up in order to determine the causes of failure. It is used to examine filler dispersion in materials, uniformity of components, agglomeration, and voids. By increasing magnification, resolution, and depth of focus [31]. Surface morphology information was obtained using Inspect^{TM}- Microscopy FEI in Baghdad, Iraq, using a scanning electron microscope (SEM) (Hitachi S-4800, Japan).

2.5 UV-Vis spectrophotometer

A Shimadzu UV-1800 UV-Vis spectrophotometer (Japan), at the College of Science, Department of Chemistry, University of Baghdad was used to examined the optical properties of the samples.

2.6 Photocatalysis

Photocatalysis by aqueous solution analysis the photocatalytic properties of Ag-WO_3/cement composite samples were evaluated under the sunlight by methylene blue (MB) degradation test. MB was used in the study to evaluate the absorption of the Ag-WO_3/cement composite in order to determine its MB dye was prepared at a concentration of 5 ppm. Samples were put into 50 mL dye solution, in a 10 cm diameter glass Petri dish and 60 minutes in a dark environment to reach the equilibrium between adsorption and desorption. Then the lighting is done under direct sunlight. The experiments were conducted on clear, sunny days between 10:00 am and 2:00 pm. The average solar irradiation intensity during the experiments was measured using a digital lux meter (Lutron LX-1010B) and ranged from 95,000 to 105,000 lux. The ambient temperature was between 32 °C and 36 °C. 3 mL aliquots were withdrawn every 10 minutes. A spectrophotometer was used to measure the absorbance of solutions with DI in order to test the absorbance of the MB solution, and the photodegradation efficiency was calculated using the absorption intensity at a wavelength of 664 nm. Water was used as a reference to track MB degradation. The percent of degradation ($D\%$) was calculated by the equation (1) [32]

$$D\% = \frac{A_0 - A}{A_0} \times 100\% \quad (1)$$

A_0 is the absorbance of initial MB, and A is the absorbance after a period of time under illumination. The measurements were repeated three times for each photocatalyst drawn from one batch of material, and the results were averaged.
The rate of degradation was found to obey (pseudo) first order kinetics and hence the degradation rate constant, k, was obtained from the first-order plot of kinetic analysis according to Eq. (2)

$$\ln \frac{A_0}{A} = kt \quad (2)$$

where k in (min^{-1}) is the unit of the photolysis rate constant

3. Results and discussion

3.1 XRD Analysis of Ag-WO_3

The X-ray diffraction (XRD) analysis of hydrated Portland cement (figure 1 (a)) reveals a distinct phase assemblage that acts as a fingerprint for its complex chemistry. The pattern is typically dominated by the strong, sharp peaks of portlandite ($Ca(OH)_2$), a key hydration product, and often shows signs of ettringite formation. A defining feature is the prominent broad hump between 24° and 38° (2θ), which is attributed to the amorphous calcium silicate hydrate (C-S-H) gel, the phase primarily responsible for the material's structural strength. It is also common to detect calcite ($CaCO_3$), which forms from the reaction of portlandite with atmospheric carbon dioxide. This combination of crystalline and amorphous components is a well-established signature, as the presence of these specific phases is consistently reported in studies analyzing cementitious matrices, such as in the work of Yang et al. [33] on photocatalytic cement composites.
Figure 1 (b) reveals the Ag-WO_3 samples crystalline structure with d-spacing of 0.3822, 0.371, and 3.65 nm, and plans of (002), (020), and (200). According to the XRD study and analysis, all the peaks are fixed at ($2\theta = 23.25$, 23.913, and 24.3), exactly correspond to the diffraction lines of monoclinic tungsten oxide (JCPDS 43-1035) [34].It is clear from the figure that silver peaks (JCPDS 04-0783) not found in the XRD pattern this due to tha small paricle size of silver less than 5 nm [35]. With increasing Ag content, no visible peaks of Ag or other phases were found in the Ag-WO_3 samples. This result indicates that the samples have good crystallinity.

3.2 UV-vis analysis of Ag-WO_3

The UV-Vis absorption spectra of the pure WO_3 and Ag-doped WO_3 nanoparticles provide clear evidence of how silver incorporation modifies the optical properties of the semiconductor. As shown in figure 2 (a), pure WO_3 displays its characteristic absorption edge within the visible light region. With the addition of silver, a distinct redshift in this absorption edge occurs, confirming that the material becomes responsive to a broader range of visible light [36]. This effect is most pronounced in the sample containing 7 wt.% Ag, suggesting an optimal doping level for enhancing light absorption. The bandgap energies were determined using Tauc plots for direct bandgap semiconductors, as

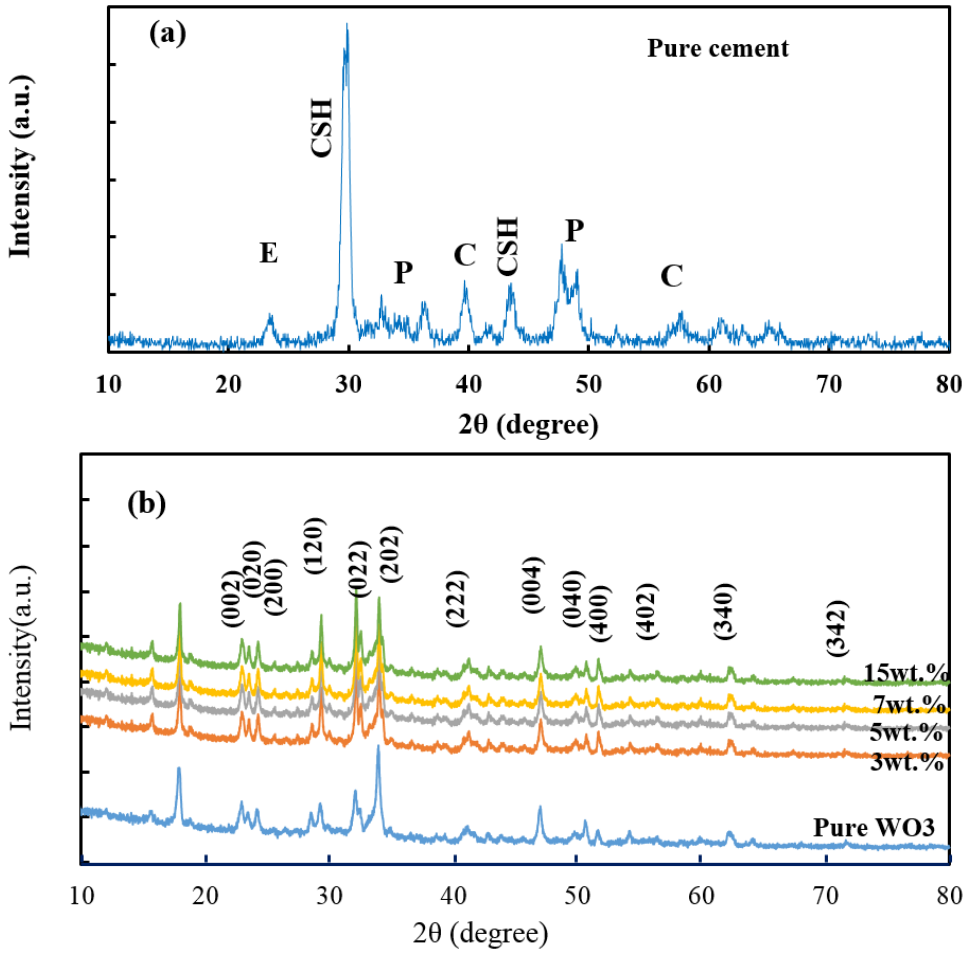

Figure 1. XRD pattern of (a) corrected pattern for pure cement, identifying Portlandite (P), Ettringite (E), and Calcite (C). The amorphous C-S-H gel is indicated. (b) Pure WO_3 and Ag-WO_3 photocatalysts with varying Ag content.

shown in figure 2 (b). The direct bandgap was calculated according to the equation:

$$(\alpha h\nu)^2 = A_0(h\nu - E_g)^n \tag{3}$$

A_0 is a constant related to fundamental band-band transitions, while ν represents the frequency of the incident photon. E_g denotes the bandgap energy value, and n is an index that reflects the type of optical transition (direct or indirect) [37]. Linear extrapolation of the rising portion of the $(\alpha h\nu)^2$ versus $h\nu$ curves to the energy axis provided the bandgap values [38].

The calculated bandgap of pure WO_3 was found to be 2.72 eV, which aligns well with established values for its monoclinic crystal structure [39]. Doping with silver significantly influenced this value, reducing the bandgap to 2.68 eV and 2.58 eV for the 5 wt.% and 7 wt.% Ag samples, respectively. This reduction is attributed to the successful integration of Ag, which introduces new energy states and promotes surface plasmon resonance effects, thereby facilitating more efficient electron excitation under visible light. In contrast, the bandgap widened to 2.75 eV for the 15 wt.% Ag sample, likely due to excessive doping causing agglomeration and

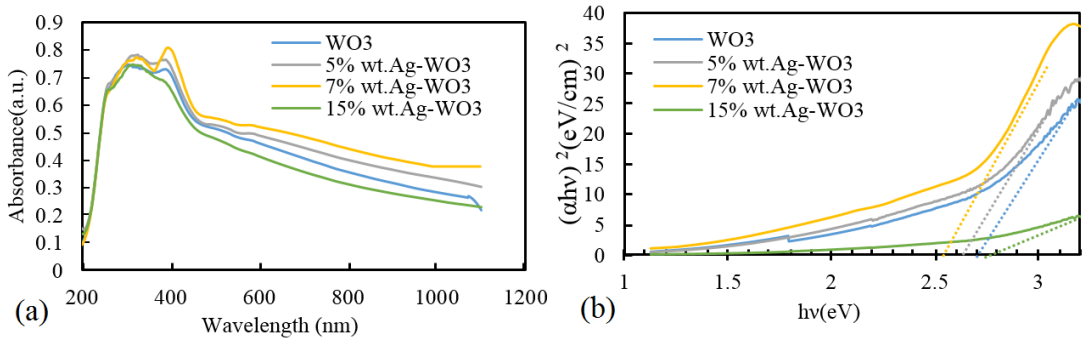

Figure 2. (a) UV-Vis absorption spectra of WO_3 and Ag-WO_3 photocatalysts; (b) Corrected Tauc plots for direct bandgap estimation. The direct bandgap (E_g).

the Burstein-Moss effect, which consequently diminishes photocatalytic performance. These optical measurements strongly support the photocatalytic activity results, confirming that the 7 wt.% Ag-WO_3 sample possesses the most favorable electronic structure for visible-light-driven degradation reactions.

3.3 Surface morphology

Scanning Electron Microscopy (SEM) was employed to examine the surface morphology and distribution of the Ag-WO_3 nanoparticles within the cement composite matrix. Figure 3 presents the SEM micrographs of composites with 7 wt.% and 15 wt.% Ag-WO_3 loadings. At the magnification used, individual WO_3 nanoparticles ($40-60$ nm) are not fully resolvable due to the integrated of these particles within the complex, micro-porous structure of the cement hydration products. However, their presence and distribution are clearly indicated by the modified surface texture and the homogeneous coverage observed across the cement particles. In the 7 wt.% Ag-WO_3 composite (figures 3 (a) and (b)), the nanoparticles appear to be well-dispersed, forming a relatively uniform coating on the cement surface. This homogeneous distribution is crucial for providing abundant active sites for photocatalytic reactions and is consistent with the superior performance of this sample [40]. Conversely, the 15 wt.% Ag-WO_3 composite (figures 3 (c) and (d)) shows clear evidence of nanoparticle agglomeration. These larger clusters reduce the effective surface area available for light absorption and pollutant adsorption. Furthermore, they can act as light-scattering centers and recombination sites for photogenerated charge carriers, explaining the significant decrease in photocatalytic efficiency observed for this sample.

3.4 Photocatalytic activity of Ag-WO_3/cement composites

The photocatalytic efficacy of the Ag-WO_3/cement composites was quantitatively assessed by tracking the photodegradation of methylene blue (MB) under solar irradiation, with the temporal evolution of the process detailed in figure 4. This figure presents the UV-Vis absorption spectra of a 5 ppm MB solution at regular intervals over a 40-minute period, with each panel corresponding to a different Ag doping percentage (0, 3, 5, 7, and 15 wt.%).
A critical observation across all spectra is the progressive diminishment of the distinct absorption maximum at 664 nm, which is directly attributable to the chromophoric structure of the MB molecule. This consistent reduction in peak intensity serves as a clear spectroscopic signature of the decomposition of MB into smaller, colourless intermediates

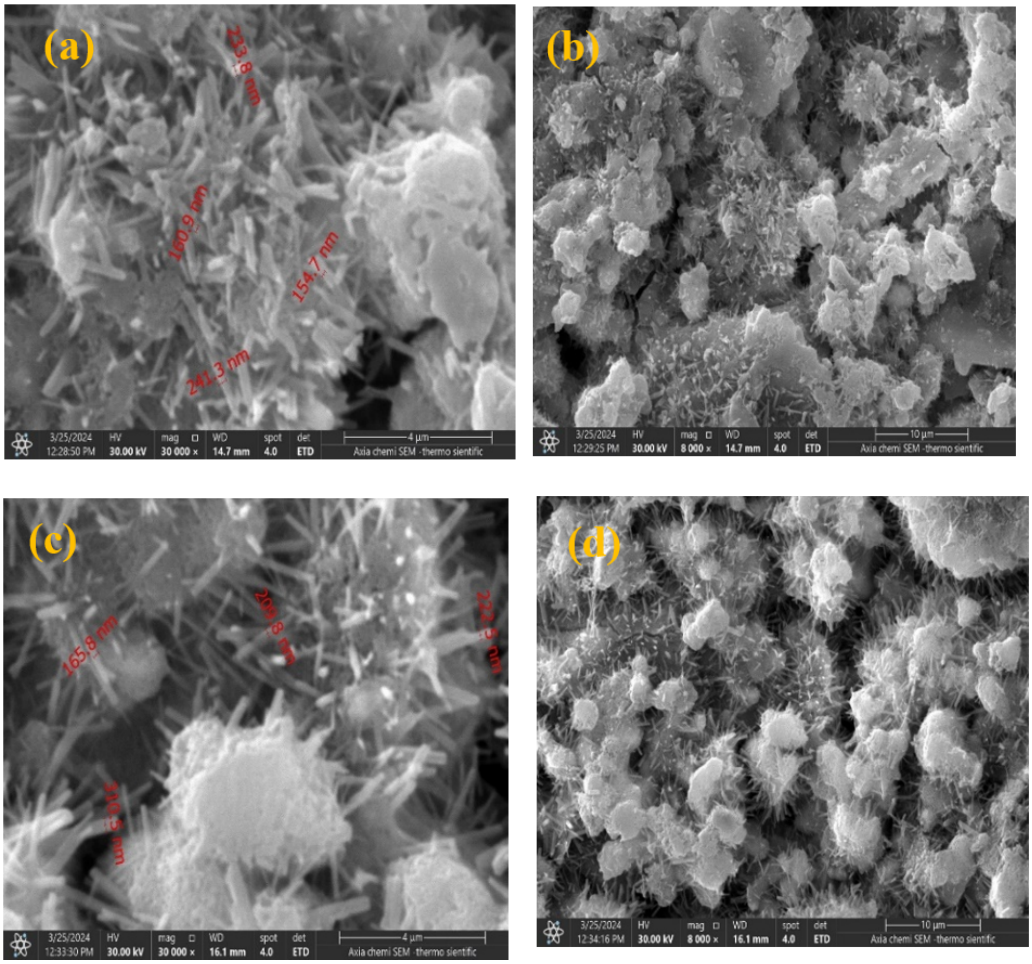

Figure 3. SEM images of Ag-WO_3/cement composites; (a, b) 7 wt.% Ag-WO_3 showing a uniform coating and dispersion; (c, d) 15 wt.% Ag-WO_3 showing areas of severe agglomeration.

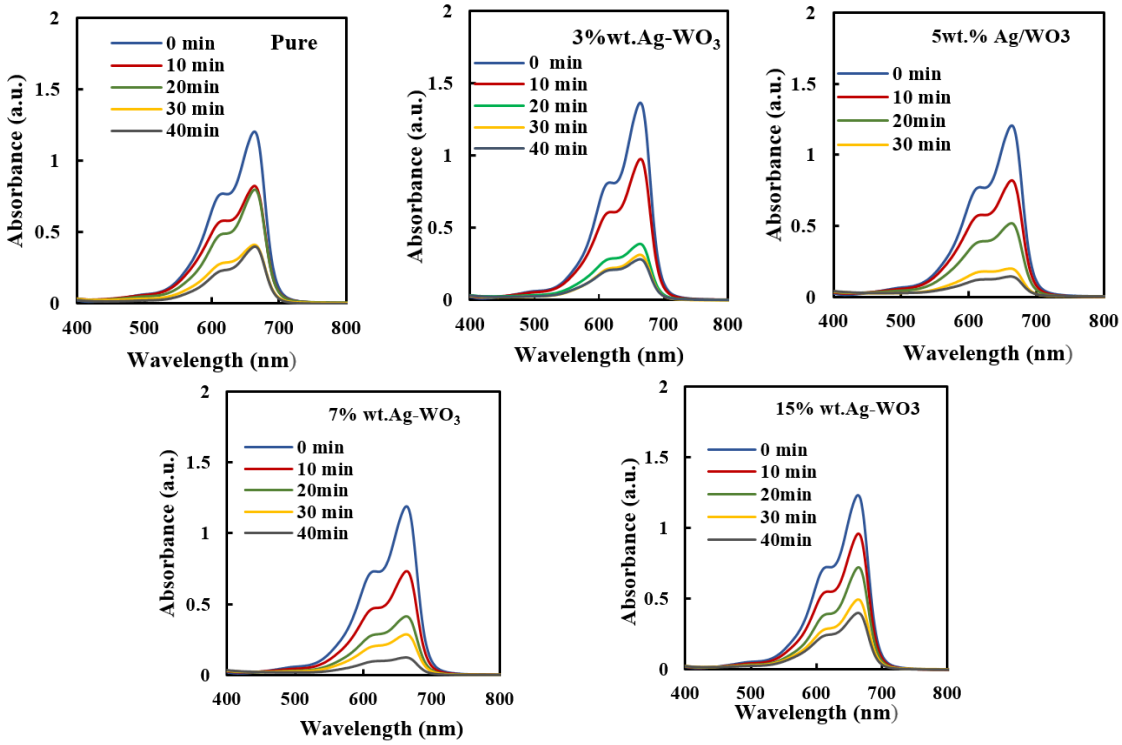

Figure 4. UV-Vis absorption spectra of photodegradation of MB dye (5 ppm) by Ag-WO_3/cement composite with different ratios.

and ultimately into mineralized end products like CO_2 and H_2O. The rate of this decay, however, is profoundly influenced by the Ag content. The composite with 7 wt.% Ag-WO_3 demonstrates the most rapid and pronounced decrease in absorbance, with the peak nearly diminishing to the baseline within the experimental timeframe. This indicates an exceptionally high efficiency in generating photogenerated charge carriers (electrons and holes) and facilitating their subsequent reactions with adsorbed species to produce oxidative radicals.

Conversely, the pure WO_3/cement sample (0 wt.%) and those with lower Ag loadings (3 and 5 wt.%) show a more gradual reduction in peak intensity. This suggests that while photocatalytic activity is present, it is sub-optimal, likely due to an insufficient number of Ag nanoparticles acting as effective electron sinks to mitigate the rapid recombination of photogenerated electron-hole pairs. Most notably, the performance of the 15 wt.% Ag-WO_3 composite reveals a counterintuitive trend: Its degradation rate is significantly slower than that of the 7 wt.% sample. This provides visual, spectroscopic evidence for the phenomenon of catalyst overload, where excessive nanoparticle loading leads to agglomeration. This agglomeration reduces the total active surface area available for both light absorption and reactant adsorption and increases light scattering, thereby impairing the overall photocatalytic efficiency. Thus, figure 4 offers direct visual confirmation that an optimal Ag concentration exists—7 wt.% in this study-which maximizes the synergistic effects between WO_3 and Ag to achieve the highest photocatalytic performance for environmental remediation applications [41].

3.5 Mechanism of MB degradation on Ag/WO_3 under sun light irradiation

The superior photocatalytic performance of the Ag-WO_3/cement composite, particularly at the optimal 7 wt.% loading, is attributed to the formation of a Schottky junction at the metal-semiconductor interface. This junction fundamentally enhances the separation and migration efficiency of photogenerated charge carriers, as illustrated in figure 5. The degradation mechanism of Methylene Blue (MB) proceeds through the following steps:

Photoexcitation and Primary Charge Separation: Under solar irradiation, photons with energy exceeding the bandgap of WO_3 (~ 2.6 eV) excite electrons (e^-) from the valence band (VB) to the conduction band (CB), generating an equal number of holes (h^+) in the VB [42].

$$WO_3 + \text{sun ligth} \rightarrow WO_3(e^-_{CB} + h^+_{VB}) \quad (4)$$

Schottky Barrier Formation and Electron Trapping: The difference in work function between silver (ϕAg ≈ 4.26 eV) and WO_3 creates a Schottky barrier at their interface. This barrier acts as an efficient electron trap, driving the rapid transfer of photogenerated electrons from the CB of WO_3 to the Ag nanoparticles. This process is critical for two reasons:

Inhibition of Charge Recombination: The spatial separation of electrons (on Ag) and holes (in WO_3) significantly reduces the rate of deleterious electron-hole recombination, thereby increasing the population of active charge carriers available for surface reactions.

Facilitation of Electron-Mediated Reactions: The accumulated electrons on the conductive Ag nanoparticles are readily available to participate in reduction reactions. They are efficiently captured by adsorbed molecular oxygen (O_2) to

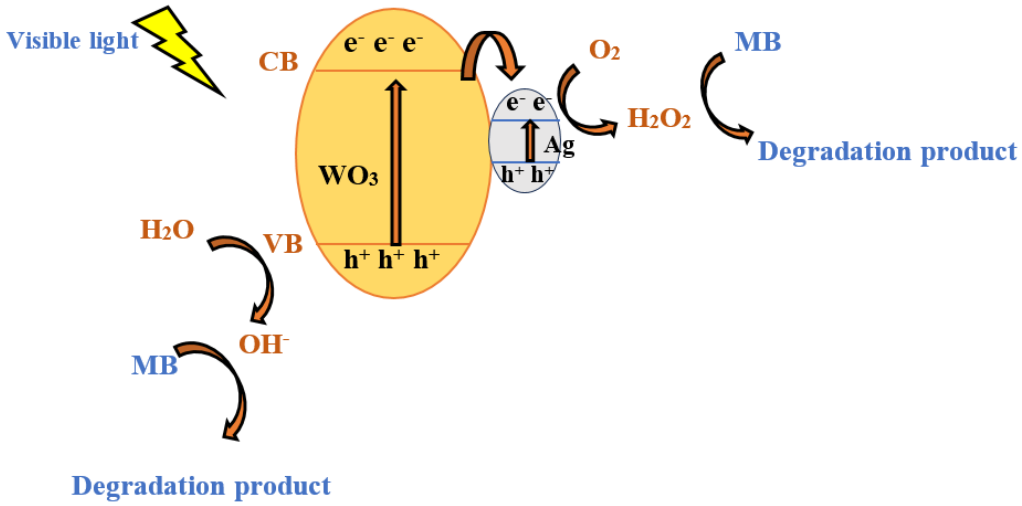

Figure 5. Mechanism of photocatalytic degradation of MB dye on Ag-WO_3/cement under sun light irradiation.

form superoxide radical anions ($^{\bullet}O_2^-$), which are primary reactive oxygen species (ROS).

$$e^- + O_2 \rightarrow {}^{\bullet}O_2^- \tag{5}$$

Generation of Reactive Oxygen Species (ROS): The superoxide radicals can undergo further reactions to generate other potent oxidants. Through protonation and multi-electron reduction pathways, hydrogen peroxide (H_2O_2) is formed, which can then be cleaved to yield highly reactive hydroxyl radicals ($^{\bullet}OH$).

$$^{\bullet}O_2^- + e^- + 2H^+ \rightarrow H_2O_2 \tag{6}$$

$$H_2O_2 + e^- \rightarrow {}^{\bullet}OH + OH^- \tag{7}$$

Concurrently, the positive holes (h^+) retained in the VB of WO_3, which possesses a highly positive potential ($\sim +3.1$ V vs. NHE), are powerful oxidants themselves. They can directly oxidize organic molecules or react with surface-adsorbed water/hydroxide ions to produce additional hydroxyl radicals.

$$h^+ + H_2O/OH^- \rightarrow {}^{\bullet}OH + H^+ \tag{8}$$

Pollutant Degradation and Mineralization: The suite of generated ROS ($^{\bullet}OH$, $^{\bullet}O_2^-$, H_2O_2) and the remaining holes (h^+) non-selectively attack the MB dye molecules. They break the chromophore structure and systematically degrade the complex organic compound into smaller, simpler organic intermediates, ultimately leading to complete mineralization into harmless products such as CO_2, H_2O, and inorganic ions.

$$ROS/h^+ + MB \rightarrow \text{Intermadiates Production} \rightarrow CO_2 + H_2O + SO_4^{2-} + NH_4/NO \tag{9}$$

Rationale for the Optimal Ag Loading (7 wt.%): This mechanistic model elucidates the observed performance peak at 7 wt.% Ag. At this optimal loading, Ag nanoparticles are well-dispersed across the WO_3 surface (as confirmed by SEM analysis), maximizing the number of effective Schottky junctions for electron trapping without compromising light absorption by WO_3. At lower Ag concentrations, the number of electron sinks is insufficient to effectively suppress charge recombination. Conversely, at excessively high loadings (e.g., 15 wt.%), Ag nanoparticles agglomerate, which reduces the effective interfacial area, shields WO_3 from light, and acts as recombination centres themselves, collectively diminishing the photocatalytic activity.

Figure 6 shows the degradation percentage of MB (5 ppm) using different Ag-WO_3/cement composites after 40 min of exposure to sunligh. According to the resultes , the sample 7% wt. Ag-WO_3 nanocomposite made dye lost 89% of its concentration during 40 minutes of irradiation. Due to increased agglomeration and lack of homogeneous dispersion in the cement material, the photodegradiation percantge decreases as the Ag-WO_3 content in the cement composite increases to 15 wt%.

Figure 7 shows the decolorization of the MB solution at different times of sunlight irradiation. After 40 minutes

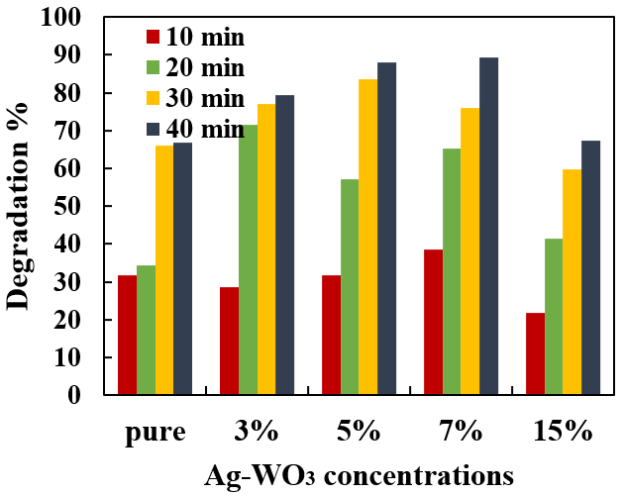

Figure 6. Photodegradation efficiency of MB dye (5ppm) by Ag-WO_3/cement composites with different ratios.

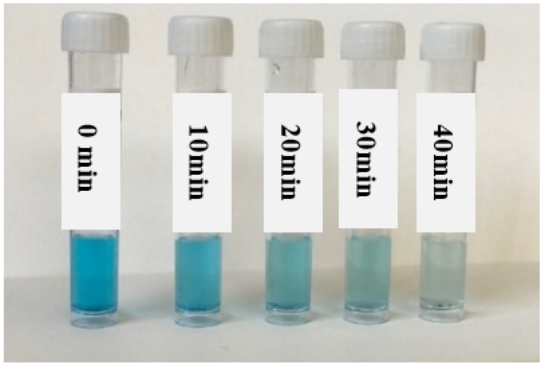

Figure 7. Decoloration of MB (5 ppm) at 7% wt. Ag-WO_3/cement composite.

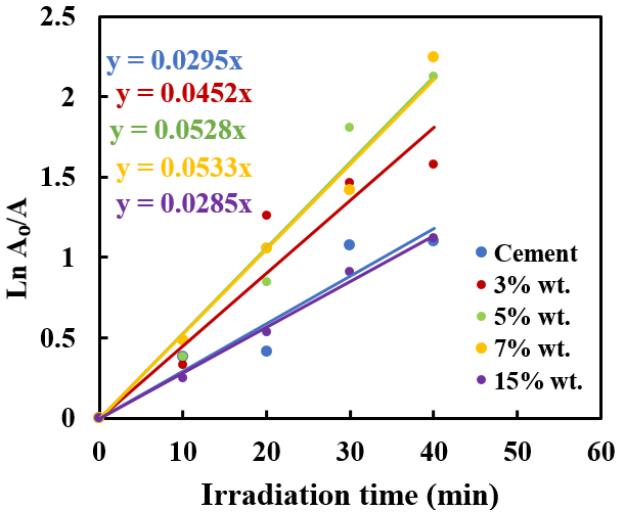

Figure 8. Relation between $\ln(A_0/A)$ versus irradiation time of MB (5 ppm) decomposition catalyzed by sunlight irradiation.

in the sun light irradiation, the color shifted from blue to light blue. Proper amount of Ag-WO_3 addition should be provided in order to eliminate unnecessary additional catalyst and achieve complete photo absorption for effective photo mineralization. It has been found that the ideal loading of the photocatalyst is affected by the initial concentration of dye solution. Pseudo-first order reaction initiates this type of reaction. When one part of a reaction present in large quantities is highly concentrated, or is maintained to the point where it is thought to remain approximately constant throughout the reaction, regardless of the concentration of the other part, it is a pseudo-first order reaction that occurs.

The liner plotting between $\ln(A_0/A)$ and time has a slope can be used to calculate the values of the rate constants (k) for photodegradations illustrated in Table 1 [43, 44], according to the graph shown in Fig. 8 & Table 1 also shows that the value of the constant (k) is 0.0533 min^{-1} for the best sample which is 7 wt.%. Once the Ag-WO_3 reached a concentration of 15 wt.%, rate constant was reduced to 0.0285 (min^{-1}). It is clear from the data that at a concentration of 7 wt.%, the degradation rate of methylene blue dye was faster.

4. Conclusion

This research successfully demonstrates that embedding 7 wt.% Ag-WO_3 nanoparticles into cement creates a highly effective, self-cleaning composite material. The optimal sample narrowed the bandgap to 2.58 eV, enabling exceptional visible-light absorption, and under natural sunlight, it degraded 89.1% of methylene blue pollutant in just 40 minutes—a reaction rate ($k = 0.0528$ min^{-1}) nearly double that of undoped cement. However, exceeding this optimal dosage to 15 wt.% caused nanoparticle agglomeration, widening the bandgap and slashing performance, highlighting a critical balance. These quantitative results confirm that the 7 wt.% Ag-WO_3/cement composite is a supremely promising material for developing smart, sustainable infrastructure that actively combat environmental pollution.

Acknowledgement

The authors would like to express their gratitude to the Department of Physics at the College of Science at the University of Baghdad for their assistance with the research.

Table 1. Rate constant (k) for different Ag-WO_3/cement composites at 5 ppm MB solution under sunlight.

Ag-WO_3 %wt.	Degradation (%) at 40 min	Rate constant (k) (min^{-1})
0	65.2% ± 2.1	0.0272 ± 0.0011
5	78.5% ± 1.8	0.0385 ± 0.0015
7	89.1% ± 1.5	0.0528 ± 0.0013
15	58.5% ± 3.0	0.0201 ± 0.0018

Authors Contribution
The intellectual substance, idea, and design of this study, or the analysis and interpretation of the data (if applicable), as well as the manuscript's writing, were all sufficiently contributed to by each author.

Availability of data and materials
The data that support the findings of this study are available from the corresponding author upon reasonable request.

Conflict of interests
The authors declare that they have no known competing financial interests or personal relationships that could have appeared to influence the work reported in this paper.

References

[1] K. U. A. Sanalkumar and E. Yang. "Self-cleaning performance of nano-TiO_2 modified metakaolin-based geopolymers.". *Cem. Concr. Compos.*, **115**:103847, 2021.

[2] L. Yang, A. Hakki, L. Zheng, M. R. Jones, F. Wang, and D. E. Macphee. "Photocatalytic concrete for NOx abatement: Supported TiO_2 efficiencies and impacts.". *Cem. Concr. Res.*, **116**:57–64, 2019.

[3] M. Z. Guo and C. S. Poon. "Superior photocatalytic NOx removal of cementitious materials prepared with white cement over ordinary Portland cement and the underlying mechanisms.". *Cem. Concr. Compos.*, **90**:42–49, 2018.

[4] P. N. María, A.-G.José Ignacio, N.-B. Iñigo, and F. A. José María. "Atmospheric NOx removal: Study of cement mortars with iron- and vanadium-doped TiO_2 as visible light-sensitive photocatalysts.". *Constr. Build. Mater.*, **149**:257–271, 2017.

[5] M. Z. Guo, T. C. Ling, and C. S. Poon. "Photocatalytic NOx degradation of concrete surface layers intermixed and spray-coated withnano-TiO_2: Influence of experimental factors.". *Cem. Concr. Compos.*, **83**: 279–289, 2017.

[6] H. Danso and I. Boateng. "Quality of type I Portland cement from Ghana and UK.". *Civil and Environmental Research*, **7**:38–47, 2015.

[7] E. C. Prada, S. G. Salgado, M. A Quijano, and F. Varela. "Controlled synthesis and microstructural properties of sol-gel TiO_2 nanoparticles for photocatalytic cement composites.". *Nanomaterials*, **9**:26–41, 2018.

[8] E. Velasco. "Scanning Electron Microscope (SEM) as a means to determine dispersibility. M.Sc. Thesis, Iowa State University Capstones.". 2013.

[9] B. B. Çırak, B. Caglar, T. Kılınç, S. M. Karadeniz, Y. Erdoğan, S. Kılıç, E. Kahveci, A. E. Ekinci, and Ç. Çırak. "Synthesis and characterization of ZnO nanorice decorated TiO_2 nanotubes for enhanced photocatalytic activity.". *Materials Research Bulletin*, **109**: 160–167, 2019.

[10] M. F. Sanad, A. E. Shalan, S. M. Bazid, and Sa. M. Abdelbasir. "Pollutant Degradation of Different Organic Dyes Using the Photocatalytic Activity of ZnO@ ZnS Nanocomposite Materials.". *Journal of Environmental Chemical Engineering*, **6**:109100, 2018.

[11] R. Sabry, M. I. Rahmah, and W. Aziz. "A Systematic Study to Evaluate Effects of Stearic Acid on Super hydrophobicity and Photocatalytic Properties of Ag- doped ZnO Nanostructures.". *Journal of Materials Science: Materials in Electronics*, **31**:109100, 2020.

[12] R. F. Kadhim. "Photocatalytic Removal of Methylene Blue Dye by Using of ZnS and CdS.". *Iraqi Journal of Physics*, **15**:109100, 2017.

[13] K.P. Devi and H. Chaturvedi. "An Overview of Nanotechnology in Water Treatment Applications and Combating Climate Change.". *Water Conservation in the Era of Global Climate Change*, page 109100, 2021.

[14] F. Zhang, X. Wang, H. Liu, C. Liu, Y. Wan, Y. Long, and Z. Cai. "Recent advances and applications of semiconductor photocatalytic.". *Technology Applied Sciences*, **9**:109100, 2019.

[15] M. R. Hoffmann, Scot T. Martin, W. Choi, and D. W. Bahnemannt. "Environmental applications of semiconductor photocatalysis.". *Chemical reviews*, **95**:69–96, 1995.

[16] S. Modi, V. K. Yadav, A. Amari, A. Y. Alyami, A.Gacem, H. N. Harharah, and M. H. Fulekar. "Photocatalytic degradation of methylene blue dye solution using different amount of ZnO as a photocatalyst.". *Science Letters*, **15**:1–12, 2021.

[17] E. Brattich, F. Barbano, B. Pulvirenti, F. Pilla, M. Bacchetti, and S. Di Sabatino. "The effect of photocatalytic coatings on NOx concentrations in real-world street canyons.". *Build. Environ*, **205**: 108312, 2021.

[18] C. Chen, B. Tang, X. Cao, F.Gu, and W. Huang. "Enhanced photocatalytic decomposition of NO on portland cement concrete pavement using nano-TiO_2 suspension". *Constr. Build. Mater.*, **275**:122135, 2021.

[19] M. Malayeri, F. Haghighat, and C. S. Lee. "Modeling of volatile organic compounds degradation by photocatalytic oxidation reactor in indoor air: A review.". *Build. Environ.*, **154**:309–323, 2019.

[20] Q. Jiang, T. Qi, T. Yang, and Y. Liu. "Ceramic tiles for photocatalytic removal of NO in indoor and outdoor air under visible light.". *Build. Environ.*, **158**:94–103, 2019.

[21] J. Xiong, L. Tian, and R. "Cheng. Promoted catalytic hydrodechlorination for deep degradation of chlorophenols over Rh-La/SiO_2 catalyst.". *Journal of Hazardous Materials*, **416**:125913, 2021.

[22] I. U. Castro, D. C. Sherrington, A. Fortuny, A. Fabregat, Fr. Stüber, J. Font, and C. Bengoa. "Synthesis of polymer-supported copper complexes and their evaluation in catalytic phenol oxidation.". *Catalysis Today*, **157**:66–70, 2010.

[23] C. Chiou, C. Wu, and R. Juang. "Influence of operating parameters on photocatalytic degradation of phenol in UV/TiO_2 process.". *Chemical Engineering Journal*, **139**:322–329, 2008.

[24] D. L. Stern and R. K. Grassell. "Propane oxydehydrogenation over molybdate-based catalysts.". *Journal of Catalysis*, **167**:550–559, 1997.

[25] M. C. Sauer, R. A. Crowell, and I. A. Shkrob. "Electron photodetachment from aqueous anions. 1. Quantum yields for generation of hydrated electron by 193 and 248 nm laser photoexcitation of miscellaneous inorganic anions.". *Journal of Physical Chemistry A*, **108**:5490–5502, 2004.

[26] C. Tossi, L. Hällström, J. Selin, M. Vaelma, E. See, J. Lahtinen, and I. Tittonen. "Size-and density-controlled photo deposition of metallic platinum nanoparticles on titanium dioxide for photocatalytic applications.". *Journal of materials chemistry A*, **7**:14519–14525, 2019.

[27] A. Hameed, M. A. Gondal, Z. H. Yamani, and A. H. Yahya. "Significance of pH measurements in photocatalytic splitting of water using 355 nm UV laser 246.". *Appl. Catal. A.*, **241**, 2001.

[28] R. S. Sabry, W. J. Aziz, and M. I. Rahmah. "Enhanced photocatalytic activity of Ag and Fe_2O_3 co-doped ZnO nanostructure under visible light irradiation.". *Materials Technology*, **35**:326–334, 2020.

[29] M. Xu, Y. Bao, K. Wu, T. Xia, H. L. Clack, H. Shi, and V. C. Li. "Influence of TiO_2 incorporation methods on NOx abatement in Engineered Cementitious Composites.". *Constr. Build. Mater.*, **221**: 375–383, 2019.

[30] A. S. Khalil, B. M. Al-Shabander, and H. M. Yaseen. "Photocatalytic activity of tetragonal $BaTiO_3$ nanoparticles prepared by wet chemical method.". *AIP Conference Procee*, **2372**:130019, 2021.

[31] S. A. Al-Lhaibi and B. M. Al-Shabander. "Study the effect of ZnO nanoparticles reinforced sawdust/epoxy composites on mechanical properties.". *Digest Journal of Nanomaterials and Biostructures*, **17**: 851–860, 2022.

[32] D. R. Paul, R. Sharma, S. P. Nehra, and A. Sharma. "Effect of calcination temperature, pH and catalyst loading on photodegradation efficiency of urea derived graphitic carbon nitride towards methylene blue dye solution.". *RSC advances*, **9**:15381–15391, 2019.

[33] M. L. Yang, A. Hakki, L. Zheng, M. R. Jones, F. Wang, and D. E. Macphee. "Photocatalytic concrete for NOx abatement: Supported TiO_2 efficiencies and impacts.". *Cem. Concr. Res.*, **116**:57–64, 2019.

[34] S. M. Harshulkhan, K. Janaki, G. Velraj, R. S. Ganapathy, and S. Krishnaraj. "Structural and optical properties of Ag doped tungsten oxide (WO_3) by microwave-assisted chemical route.". *J. Mater. Sci. Mater. Electron.*, **27**:3158–3163, 2015.

[35] T. Tomoharu, K. Tadashi, T. Kenta, N. Naohiro, H. Yasuhiko, K. Sasaki, and K. Kotaro. "Growth and Structure Analysis of Tungsten Oxide Nanorods Using Environmental TEM.". *8th International Vacuum Electron Sources Conference and Nanocarbon, IEEE*, 2010.

[36] M. Khan, S. Kumar, T. Ahamad, and A. Alhazaa. "Enhancement of photocatalytic and electrochemical properties of hydrothermally synthesized WO_3 nanoparticles via Ag loading.". *J. Alloys Compd.*, **743**, 2018.

[37] H. Najafi-Ashtiani, A. Bahari, S. Gholipour, and S. Hoseinzadeh. "Structural, optical and electrical properties of WO_3–Ag nanocomposites for the electro-optical devices.". *Appl. Phys. A*, **124**:24, 2017.

[38] P. Hua-Feng, X. Xiang, Z. Li, Y. Q. Fu, and X.-T. Zu. "Hydrothermal synthesis and optical properties of hexagonal tungsten oxide nanocrystals assisted by ammonium tartrate.". *Phys. Status Solidi*, **209**:537–544, 2012.

[39] M. Desseigne, N. Dirany, V. Chevallier, and M. Arab. "Shape dependence of photosensitive properties of WO_3 oxide for photocatalysis under solar light irradiation.". *Appl. Surf. Sci.*, **483**:311–323, 2019.

[40] Mo. Shokri, A. Jodat, N. Modirshahla, and M. A. Behnajady. "Photocatalytic degradation of chloramphenicol in an aqueous suspension of silver-doped TiO_2 nanoparticles.". *Environmental Technology*, **34**: 1161–1166, 2013.

[41] P. Dong, B. Yang, C. Liu, F. Xu, X. Xi, G. Hou, and R. Shao. "Highly enhanced photocatalytic activity of WO_3 thin films loaded with Pt–Ag bimetallic alloy nanoparticles.". *RSC Adv.*, **7**:947–956, 2017.

[42] S. A. Al-Lhaibi and B. M. Al-Shabander. "Photocatalytic Activity and Wettability Properties of ZnO/Sawdust/Epoxy Composites.". *Iraqi Journal of Physics*, **1**:54–65, 2022.

[43] M. Sethi. "Magnesium Oxide Nanostructures: Synthesis, Characterization and Environmental Application. M.Sc. Thesis, national institute of technology, Rourkela.". 2014.

[44] A. L. T. Zheng, C. A. C. Abdullah, E. L. T. Chung, and Y. Andou. "Recent progress in visible light-doped ZnO photocatalyst for pollution control.". *Inter. J. Env Sci. and Tech.*, **20**:5753–5772, 2023.